Separable potential model for meson-baryon interaction beyond the *S* wave

Vojtěch Krejčiřík*

Maryland Center for Fundamental Physics, Department of Physics, University of Maryland, College Park, Maryland 20742-4111, USA

(Received 5 July 2012; published 23 August 2012)

A model for low-energy meson-baryon interaction in the strange sector is presented. The interaction is described in terms of separable potentials with multiple partial waves considered. A general solution of the Lippmann-Schwinger equation for the scattering of spin-0 and spin-1/2 particles is derived. Next, the general framework is applied to the $\overline{K}N$ sector in a simple model with only the S and P waves taken into account. The separable potential is designed to match the chiral perturbation theory at the lowest nontrivial order. It is shown that although a simple model with three free parameters works well for the S wave, it fails to reproduce the P-wave features of kaon-nucleon physics. Most importantly, the P-wave interaction is too weak to express a resonant behavior that could be identified as $\Sigma(1385)$ resonance.

DOI: 10.1103/PhysRevC.86.024003 PACS number(s): 11.80.Gw, 12.38.Lg, 12.39.Fe, 13.75.Jz

I. INTRODUCTION

The description of low-energy meson-baryon interaction in the strange sector is a highly puzzling problem. The direct application of the effective theory approach [1], which was successful in the pion-nucleon sector, i.e., baryonic chiral perturbation theory (for review, see Ref. [2]), is problematic. The key physical issue is the presence of the $\Lambda(1405)$ resonance below the $\overline{K}$-N threshold [3]. The existence of a resonance implies the need to work to all orders in perturbation theory and therefore procedures alternative to standard chiral perturbation theory (χPT) are required.

A possible way to proceed is via the multichannel Lippmann-Schwinger equation with the interaction described by separable potentials [4–6]. The physics based on chiral symmetry of QCD is reflected in the design of the respective separable potentials. They are designed to match the amplitudes obtained in chiral perturbation theory up to given order $O(p^n)$. In the hypothetical world of very low quark masses, amplitudes obtained by iterating the Lippmann-Schwinger equation with such potentials are equal to the amplitudes derived in χPT up to a given order in the chiral expansion $O(p^n)$. Note that the χPT is constructed as an effective theory of QCD in the regime of low momenta and low quark masses. However, in the physical world with a relatively high s quark mass, the connection to the fundamental theory of strong interactions—the QCD—is more subtle.

The suggested approach has, on the other hand, the advantage that the Lippmann-Schwinger equation is exactly solvable; the originally complicated system of coupled integral equations simplifies to an algebraic equation and a set of integrals. Additionally, some features of nuclear medium, for example, Pauli blocking [7] and/or self-energy effects [8], can be straightforwardly incorporated into the separable potential model. Kaon-nucleon amplitudes enriched with in-medium effects may then be used to determine an effective in-medium kaon-nuclear potential [9,10], as well as to study other low-energy processes involving kaon-nuclear interaction, for example, the hypernuclear production [11,12].

In their recent work, Cieplý and Smejkal [6,10] were able to fit a large set of low-energy experimental data (threshold branching ratios, kaonic hydrogen shift and width, and cross sections to various channels for kaon incident momentum up to 200 MeV) with a very simple model combining the chiral dynamics with a separable potential approach considering only the $L = 0$ partial wave. They were also able to analyze the properties of the $\Lambda(1405)$ resonance. However, the model of Ref. [6] has an important limitation—it considers only the S-wave contribution. Although this turned out to be sufficient for the kaon incident momentum up to 200 MeV, the inclusion of higher partial waves becomes necessary if one wants to go to higher kaon momenta. Moreover, the P-wave interaction is expected to play an important role in the formation of deeply bound K^--nuclear states [13,14]. Although the authors of Ref. [14] used the more fundamental model of Ref. [10] for the S-wave interaction, they relied on purely phenomenological parametrization for the P-wave interaction. Thus, the improvement of the understanding of the P-wave part of meson-baryon interactions in the strange sector is certainly desirable.

The goal of this paper is to extend the separable potential model of Ref. [6] for meson-baryon interactions in the strange sector to include the effects of the P wave. With the P-wave part included in the separable potential, one should gain access to phenomena which are inaccessible if only the S wave is included, for example, the angular distribution of the cross section. Moreover, one might expect that the P-wave resonance $\Sigma(1385)$ could be dynamically generated using the P-wave potential in a way similar to that for the $\Lambda(1405)$ resonance, as was studied by Cieplý and Smejkal.

The paper is organized as follows. The general formalism of spin-0 spin-1/2 particle scattering is summarized in Sec. II. In Sec. III, the general form for a multichannel separable potential model is discussed and the solution of the Lippmann-Schwinger equation is derived for such potentials. In Sec. IV, the potential for kaon-proton scattering is constructed to match the χPT up to the lowest nontrivial order. Fits to the

*vkrejcir@umd.edu

available experimental data and discussion of the obtained results follows in Sec. V.

II. FORMALISM OF SPIN0 SPIN-1/2 SCATTERING

In this section, the formalism describing two-particle scattering—one with spin-1/2 and one with spin0—is summarized. To be concrete, only the interactions that are both time-reversal and parity invariant are considered; all formulas are given in the center-of-mass frame of reference.

The most general form of the scattering amplitude is a 2×2 spin matrix [15]:

$$\mathbf{f}(\mathbf{p} \to \mathbf{p}') = \tilde{f}(\mathbf{p} \to \mathbf{p}') + i\,\sigma \cdot \hat{\mathbf{p}} \times \hat{\mathbf{p}}'\ \tilde{g}(\mathbf{p} \to \mathbf{p}'). \quad (1)$$

In Eq. (1), $\mathbf{p}$ and $\mathbf{p}'$ stand for the initial and final center-of-mass momentum. A hat above a vector indicates a unit vector in the respective direction. The spin nonflip and spin flip amplitudes are denoted as $\tilde{f}$ and $\tilde{g}$.

Due to parity invariance, the total angular momentum J and the orbital angular momentum L are separately conserved during the scattering. Thus, for a given initial orbital momentum L (a given partial wave), there are two independent S-matrix elements—one for $J = L + 1/2$ and one for $J = L - 1/2$—that fully characterize the scattering process. Therefore, one can write down the generalized partial wave expansion using the projection operators into the respective subspaces $J = L \pm 1/2$. The amplitude reads

$$\mathbf{f}(\mathbf{p} \to \mathbf{p}') = \sum_L (2L+1)[f^{L+}(\mathbf{p} \to \mathbf{p}')\,\Lambda^{L+} + f^{L-}(\mathbf{p} \to \mathbf{p}')\,\Lambda^{L-}]P_L(\hat{\mathbf{p}} \cdot \hat{\mathbf{p}}'), \quad (2)$$

where $\Lambda^{L\pm}$ is a projection operator to a subspace of total angular momentum $J = L \pm 1/2$:

$$\Lambda^{L+} = \frac{1}{2L+1}(L+1+\sigma \cdot \mathbf{L}), \quad \Lambda^{L-} = \frac{1}{2L+1}(L-\sigma \cdot \mathbf{L}).$$

Simple algebraic manipulations allow one to find a partial wave expansion for spin flip and spin nonflip amplitudes ($\tilde{f}$ and $\tilde{g}$) in terms of amplitude projections for given total and orbital angular momenta (f^{L+}, f^{L-}):

$$\tilde{f} = \sum_L [(L+1)\,f^{L+} + L\,f^{L-}]P_L(\hat{\mathbf{p}} \cdot \hat{\mathbf{p}}'), \quad (3)$$

$$\tilde{g} = \sum_L [f^{L+} - f^{L-}]P'_L(\hat{\mathbf{p}} \cdot \hat{\mathbf{p}}'). \quad (4)$$

Note that if the spin-orbit coupling is zero, amplitude f^{L+} is equal to f^{L-}. In this case, the partial wave expansion for spin nonflip amplitude $\tilde{f}$ coincides with the standard one for the scattering of two spinless particles and the spin flip amplitude $\tilde{g}$ vanishes.

In this parametrization, the differential cross section for the unpolarized beam and target reads

$$\frac{d\sigma}{d\Omega}(\mathbf{p} \to \mathbf{p}') = |\tilde{f}(\mathbf{p} \to \mathbf{p}')|^2 + \sin^2(\theta)\ |\tilde{g}(\mathbf{p} \to \mathbf{p}')|^2. \quad (5)$$

If only $L = 0$ and $L = 1$ are included—the model which will be investigated later in the paper—the differential and total cross sections read as follows:

$$\frac{d\sigma}{d\Omega} = (|f^{0+}|^2 + |2f^{1+} + f^{1-}|^2\cos^2\theta + |f^{1+} - f^{1-}|^2\sin^2\theta + [f^{0+}(2f^{1+} + f^{1-})^* + (f^{0+})^*(2f^{1+} + f^{1-})]\cos\theta), \quad (6)$$

$$\sigma^{\text{tot}} = 2\pi\left(2|f^{0+}|^2 + \frac{2}{3}|2f^{1+} + f^{1-}|^2 + \frac{4}{3}|f^{1+} - f^{1-}|^2\right). \quad (7)$$

The angular distribution of the differential cross section is often parametrized in powers of $\cos\theta$:

$$\frac{d\sigma}{d\Omega} \approx A_0 + A_1\cos\theta + A_2\cos^2\theta + \cdots, \quad (8)$$

$$A_0 = |f^{0+}|^2 + |f^{1+} - f^{1-}|^2,$$
$$A_1 = 2\,\text{Re}[f^{0+}(2f^{1+} + f^{1-})],$$
$$A_2 = |2f^{1+} + f^{1-}|^2 - |f^{1+} - f^{1-}|^2. \quad (9)$$

Note that A_0, A_1, and A_2 are the only three coefficients that are nonzero if only S and P waves are considered.

III. SEPARABLE POTENTIALS AND A SOLUTION OF THE LIPPMANN-SCHWINGER EQUATION

In this section, a general form of a multichannel separable potential between spin-1/2 and spin-0 particles is discussed. It is shown that, even in this relatively complicated case, the solution of a Lippmann-Schwinger equation simplifies to an algebraic problem. To cover the most general situation when particle types can change during the process, the multichannel approach to the problem is employed from the beginning; individual channels are labeled (ai), where a stands for the type of spin-1/2 particle (baryon) and i stands for the spin-0 particle (meson).

Knowing the general form of the scattering amplitude (2), the potential is taken to have the following form:

$$V_{(ai)\to(bj)}(\mathbf{p} \to \mathbf{p}') = \sum_L (2L+1)\left(V^{L+}_{(ai)\to(bj)}\Lambda^{L+} + V^{L-}_{(ai)\to(bj)}\Lambda^{L-}\right) \times P_L(\hat{\mathbf{p}} \cdot \hat{\mathbf{p}}')\,g^L_{(ai)}(p)\,g^L_{(bj)}(p'), \quad (10)$$

where $g^L_{(ai)}(p)$ is a form factor corresponding to the channel (ai) and the partial wave L.

The Lippmann-Schwinger equation reads

$$T_{(ai)\to(bj)}(\mathbf{p} \to \mathbf{p}') = V_{(ai)\to(bj)}(\mathbf{p} \to \mathbf{p}') + \sum_{(ck)} 2\mu_{(ck)}\int d^3q\,\frac{V_{(ai)\to(ck)}(\mathbf{p} \to \mathbf{q})\,T_{(ck)\to(bj)}(\mathbf{q} \to \mathbf{p}')}{p^2_{(ck)} - q^2 + i\epsilon}, \quad (11)$$

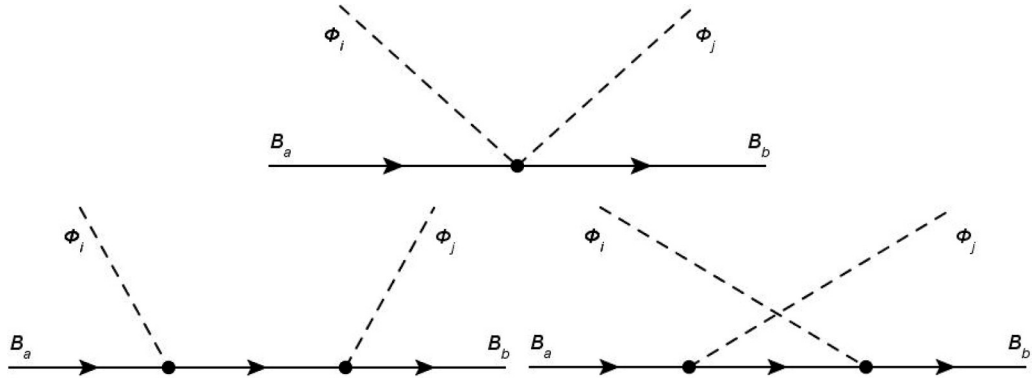

FIG. 1. Feynman diagrams representing the Weinberg-Tomozawa, direct (s-channel), and crossed (u-channel) contributions to the meson-baryon scattering.

where the sum is over all possible intermediate channels (ck), $p_{(ck)}$ is the on-shell momentum in the intermediate channel, and $\mu_{(ck)}$ is its reduced energy.

Having the potential in the separable form (10), it is natural to use the following ansatz for the T matrix:

$$T_{(ai)\to(bj)}(\mathbf{p}\to\mathbf{p}') = \sum_L (2L+1)\left(T^{L+}_{(ai)\to(bj)}\Lambda^{L+} + T^{L-}_{(ai)\to(bj)}\Lambda^{L-}\right) \times P_L(\hat{\mathbf{p}}\cdot\hat{\mathbf{p}}')\, g^L_{(ai)}(p)\, g^L_{(bj)}(p'). \quad (12)$$

To prove that the separable potential (10) and the T-matrix ansatz (12) actually transform the Lippmann-Scwhinger equation into an algebraic equation, the crucial thing is to show that the integral in Eq. (11) actually splits into two pieces, one for $J = L + 1/2$ and one for $J = L - 1/2$, and preserves the separability for each piece. The separation of the angular and radial parts of the integral gives

$$\sum_{LL'}\sum_{(ck)} 2\mu_{(ck)} \int dq q^2 \frac{(2L+1)(2L'+1)}{p^2_{(ck)} - q^2 + i\epsilon} \times g^L_{(ai)}(p)\, g^L_{(ck)}(q)\, g^{L'}_{(ck)}(q)\, g^{L'}_{(bj)}(p') \times \int d\Omega_{\mathbf{q}} \left(V^{L+}_{(ai)\to(ck)}\Lambda^{L+} + V^{L-}_{(ai)\to(ck)}\Lambda^{L-}\right) P_L(\hat{\mathbf{p}}\cdot\hat{\mathbf{q}}) \times \left(T^{L'+}_{(ck)\to(bj)}\Lambda^{L'+} + T^{L'-}_{(ck)\to(bj)}\Lambda^{L'-}\right) P_{L'}(\hat{\mathbf{q}}\cdot\hat{\mathbf{p}}').$$

The orthogonality of Legendre polynomials and the properties of projection operators are key ingredients in the proof of separability. Finally, one gets two independent sets of matrix equations in the channel space, one for $J = L + 1/2$ and one for $J = L - 1/2$:

$$T^{L\pm}_{(ai)\to(bj)} = V^{L\pm}_{(ai)\to(bj)} + V^{L\pm}_{(ai)\to(ck)} G^L_{(ck)} T^{L\pm}_{(ck)\to(bj)}. \quad (13)$$

G^L is a diagonal matrix with elements given by the integral:

$$G^L_{(ck)} = 4\pi\mu_{(ck)} \int \mathrm{d}q\, q^2 \frac{\left[g^L_{(ck)}(q)\right]^2}{p^2_{(ck)} - q^2 + i\epsilon}. \quad (14)$$

The relation between the T-matrix elements $T^{L\pm}_{(ai)\to(bj)}$ and the scattering amplitudes $f^{\pm}_{(ai)\to(bj)}$ is

$$f_{(ai)\to(bj)} = -4\pi\sqrt{\mu_{(ai)}\mu_{(bj)}}\, T_{(ai)\to(bj)}. \quad (15)$$

From here one straightforwardly obtains all the information about the scattering process using formulas derived in the previous section.

In the case with only S and P waves considered, the potential is of the following form:

$$V_{(ai)\to(bj)} = V^{0+} g^0_{(ai)} g^0_{(bj)} + 3(V^{1+}\Lambda^{1+} + V^{1-}\Lambda^{1-}) g^1_{(ai)} g^1_{(bj)}$$
$$\cos\theta = V^{0+} g^0_{(ai)} g^0_{(bj)} + [(2V^{1+} + V^{1-})\cos\theta + (V^{1+} - V^{1-}) i\sigma\cdot\hat{\mathbf{p}}\times\hat{\mathbf{p}}'] g^1_{(ai)} g^1_{(bj)}. \quad (16)$$

Analogous expansions hold for the T-matrix and the scattering amplitude as well. Overall, there are three independent equations of the form of Eq. (13) for T^{0+}, T^{1+}, and T^{1-}.

IV. THE CONSTRUCTION OF SEPARABLE POTENTIALS FOR KAON-PROTON SCATTERING

The separable potential (16) used in the calculation will be constructed to match the χPT up to order $O(p)$, the lowest nontrivial order, in this section. Thus, a brief review of relevant parts of the baryon χPT is in order.

The first-order chiral Lagrangian [16] reads

$$\mathcal{L}^{(1)} = i\langle\overline{B}\gamma_\mu[D^\mu, B]\rangle - M_0\langle\overline{B}B\rangle - \frac{D}{2}\langle\overline{B}\gamma_\mu\gamma_5\{u^\mu, B\}\rangle - \frac{F}{2}\langle\overline{B}\gamma_\mu\gamma_5[u^\mu, B]\rangle. \quad (17)$$

For meson-baryon scattering, one gets three principally different contributions from the diagrams summarized in Fig. 1. The first one represents the contact interaction coming from the $O(p^1)$ Lagrangian, the so-called Weinberg-Tomozawa term (WT); it is a leading contribution to the S-wave amplitudes. The other two diagrams correspond to the direct (s-channel) and crossed (u-channel) processes built from vertexes from the $O(p^1)$ Lagrangian. At first sight, these seem to be of order $O(p^2)$. However, the nonrelativistic baryon propagator $1/k^0$ is of order $O(p^{-1})$ making the leading behavior of the diagram be $O(p^1)$. These diagrams represent the leading-order contribution to the P-wave amplitudes. Some of the amplitudes may be found in the literature [16–19], and all of them can be reconstructed from the potentials presented below.

TABLE I. Kaon-nucleon threshold data.

	Fit	Exp. [21,22]
γ	2.36	2.36 ± 0.04
R_c	0.637	0.664 ± 0.011
R_n	0.178	0.189 ± 0.015
ΔE	−296 eV	-283 ± 42 eV
Γ	761 eV	541 ± 111 eV

The separable potentials (16) are constructed to match the chiral perturbation theory:

$$V_{(ai)\to(bj)} = \frac{1}{4(2\pi)^3}\sqrt{\frac{1}{s\mu_{(ai)}\mu_{(bj)}}}\,\mathcal{M}_{(ai)\to(bj)}, \tag{18}$$

where $\mathcal{M}_{(ai)\to(bj)}$ are Lorenz invariant scattering amplitudes obtained in χPT up to a given order $O(p^n)$; only the leading order $O(p^1)$ is considered in this paper.

Because the S and P waves are considered in the model, two form factors are needed; one for $L = 0$ and one for $L = 1$. For simplicity, Yamaguchi-type form factors [20] are used in the following calculation:

$$g^0_{(ai)}(p) = \frac{1}{1+\frac{p^2}{\alpha^2_{(ai)}}}, \tag{19}$$

$$g^1_{(ai)}(p) = \frac{p}{\left(1+\frac{p^2}{\alpha^2_{(ai)}}\right)^{3/2}}, \tag{20}$$

where $\alpha_{(ai)}$ characterizes the range of the interaction in the particular channel.

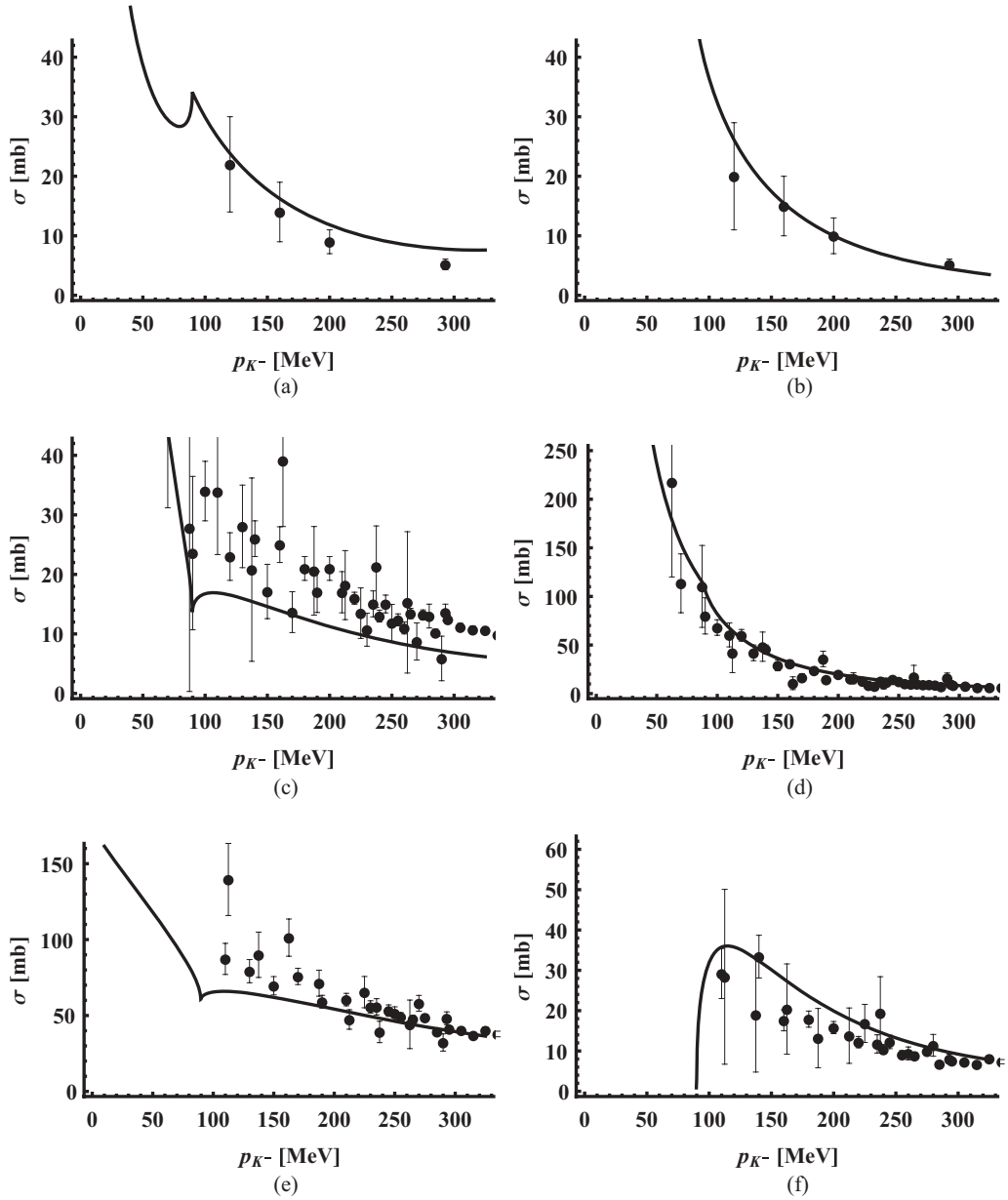

FIG. 2. The total cross section for channels $\pi^0\Lambda$ (a), $\pi^0\Sigma^0$ (b), $\pi^-\Sigma^+$ (c), $\pi^+\Sigma^-$ (d), K^-p (e), and $\overline{K}^0 n$ (f). Experimental data are from Refs. [23–29].

The use of Eqs. (16), (18)–(20) immediately leads to the potentials $V^{L\pm}$. Recall that, for the $L = 1$ part, the one power of the momentum p (p') is already included in the form factor $g^1_{(ai)}(p)$ (20) and therefore does not appear in the respective potentials V^{1+} (22) and V^{1-} (23). The potentials up to order $O(p^1)$ read as follows:

$$V^{0+}_{(ai)\to(bj)} = \mathcal{N}\left[-\frac{1}{8}\left(E_i + \frac{E_i^2 - m_i^2}{2M_i^2} + E_j + \frac{E_j^2 - m_j^2}{2M_j^2}\right) \times \mathcal{C}^{\rm WT}_{(ai)\to(bj)}\right], \tag{21}$$

$$V^{1+}_{(ai)\to(bj)} = \mathcal{N}\left[-\frac{1}{9}\left(\frac{1}{m_i + m_j}\right)\mathcal{C}^{\rm crossed}_{(ai)\to(bj)}\right], \tag{22}$$

$$V^{1-}_{(ai)\to(bj)} = \mathcal{N}\left[\frac{1}{6}\left(\frac{1}{m_i + m_j}\right)\mathcal{C}^{\rm direct}_{(ai)\to(bj)} + \frac{1}{18}\left(\frac{1}{m_i + m_j}\right) \times \mathcal{C}^{\rm crossed}_{(ai)\to(bj)}\right]. \tag{23}$$

The constant $\mathcal{N}$ guaranteeing proper relativistic flux normalization reads as follows:

$$\mathcal{N} = \frac{1}{2f_\pi^2}\frac{1}{(2\pi)^2}\sqrt{\frac{M_a M_b}{s\mu_{(ai)}\mu_{(bj)}}}. \tag{24}$$

Matrices $\mathcal{C}^{\cdots}$ are summarized in the Appendix. They determine how the channels are coupled between each other.

A brief comment about the $V^{1\pm}$ potentials is in order. In the leading-order amplitude in χPT, there is a sum of meson energies $E_i + E_j$ in the denominator. However, it leads to a possible unphysical divergence in the deep subthreshold region. This divergence is trackable back to the form of the fully relativistic baryon propagator, which diverges for $k_\mu k^\mu = -M^2$. The complication here is due to the fact that the calculation is restricted solely to the tree diagrams at the level of χPT. This divergence, eventually, disappears if one continues to higher orders. In the presented model, the spurious divergence is avoided by replacing the meson energy E_i by meson mass m_i wherever it appears in the denominator, as was suggested in Ref. [10].

The potential for the S-wave V^{0+} part is identical to the leading part of the potential used by Cieplý and Smejkal [6] and Kaiser *et al.* [4]. The P-wave contributions V^{1+} and V^{1-} have not been considered by these authors.

V. FIT TO THE LOW-ENERGY K^--P DATA AND DISCUSSION OF THE OBTAINED RESULTS

The comparison of the chirally motivated separable potential model from the previous section to the experimental low-energy data is presented and discussed here. The model developed in the previous section contains, in its full complexity, a substantial number of free parameters. For example, there are in principle 20 different inverse range parameters $\alpha^{0,1}_{(ai)}$ characterizing form factors $g^{0,1}_{(ai)}(p)$. More parameters would appear if one considers the second-order chiral Lagrangian. However, it is useful to keep the analysis simple and straightforward. Thus, the model is restricted to the first-order chiral Lagrangian and the same inverse range parameter is used for all channels: α^S for the S-wave form factors (19) and α^P for the P-wave form factors (20). In the leading-order χPT, the decay constant f_π is the same for all mesons in the pseudoscalar octet (pions, kaons, η); its value is not constrained experimentally and is thus subject to fit. Overall, there are three free parameters to be specified: inverse ranges α^S and α^P, and f_π controlling the strength of the interaction.

From the point of view of the partial wave analysis, the low-energy experimental data may be divided into three subcategories. First, the threshold branching ratios [21] and kaonic hydrogen properties [22] are influenced entirely by the S-wave physics. Cross sections are influenced by both S and P waves (and, naturally, higher partial waves as the energy of the collision increases), yet they are nonzero even if the P wave is neglected. And finally, properties of the angular distribution of the differential cross sections require the presence of the P wave. All of them are considered in the analysis. Because the $\Lambda(1520)$ resonance, which is a D wave resonance, emerges at the kaon incident momentum around 400 MeV, the validity of the model containing only S and P waves is certainly limited to below this value; this paper considers only the scattering data up to 300 MeV [23–29], because there is a significant effect of the P wave while the effect of the D wave is expected to be negligible. The

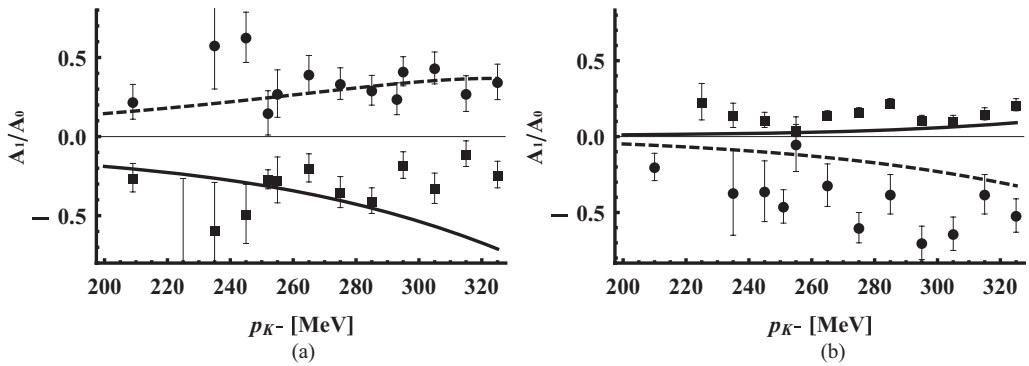

FIG. 3. Asymmetries A_1/A_0 in the differential cross sections. Channels $\pi^-\Sigma^+$ (solid line, squares) and $\pi^+\Sigma^-$ (dashed line, circles) are in graph (a); channels K^-p (solid line, squares) and $\overline{K}^0 n$ (dashed line, circles) are in graph (b).

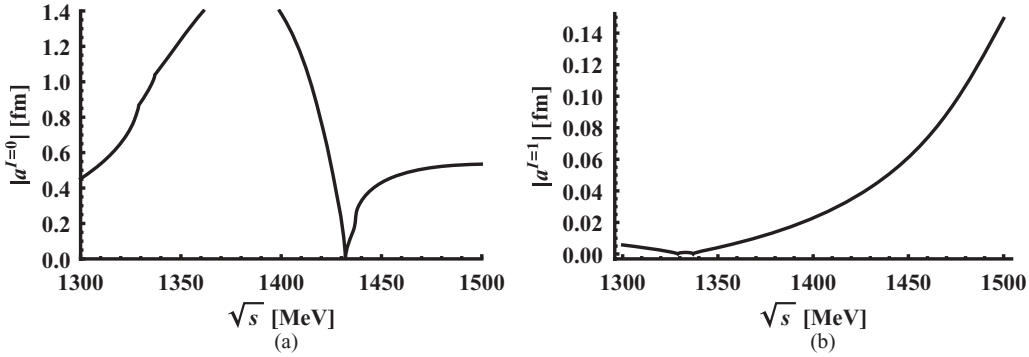

FIG. 4. Absolute values of isoscalar $\pi\Sigma$ amplitudes for 0^+ (a) and isovector $\pi\Sigma$ amplitude for 1^+ (b) partial waves.

key novelty of this paper is the focus on the effects of the P-wave interaction; therefore the attention is given to angular distribution of the differential cross section. The asymmetry in the angular distribution, which is parametrized by the quantity A_1/A_0 (9), begins to be observable at kaon incident momenta above 200 MeV [23,24,27,28]. The experimental data on angular distributions are, unfortunately, very imprecise and available only for channels $\pi^-\Sigma^+$, $\pi^+\Sigma^-$, K^-p, and $\overline{K}^0n$.

In the fitting of free parameters, a simple minimization of χ^2 is problematic; the χ^2 fit weights most importantly the data points that are most precise. In this case, the threshold branching ratios, whose uncertainties are orders of magnitude smaller than the uncertainties of other data points, would dominate the fit, whereas the properties of angular distribution, which depend dominantly on P-wave physics, would be almost irrelevant because their uncertainties are big. Because the main focus of this paper is the P-wave interaction, the following procedure, which emphasizes the P-wave physics, is adopted. First, the threshold characteristics and total cross section at low kaon momenta (at 100 MeV for $\pi^-\Sigma^+$ and $\pi^+\Sigma^-$, at 110 MeV for K^-p and $\overline{K}^0n$, and at 120 MeV for $\pi^0\Lambda$ and $\pi^0\Sigma^0$) are fitted with only the S-wave interaction taken into account. It is justified by the fact that the P-wave interaction is negligible for such low energies. In this procedure, the free parameters controlling the S-wave interaction, α^S and f_π, are set. Next, with the S-wave potential fixed, the total cross sections at higher kaon momentum (300 MeV for all channels) and asymmetries in the angular distribution (A_1/A_0 for momenta 225, 250, 275, and 300 MeV for channels $\pi^-\Sigma^+$, $\pi^+\Sigma^-$, K^-p, and $\overline{K}^0n$) are fitted with full potential to get the α^P.

The best results were obtained for the following values of free parameters: $\alpha^S = 736\,\text{MeV}$, $f_\pi = 116.6\,\text{MeV}$, and $\alpha^P = 1353\,\text{MeV}$; the overall $\chi^2/N = 4.3$. The fact that the χ^2/N is well above 1 is not a problem because the presented model does not aspire to be the complete description of nature. The comparison with experimental data is summarized in Table I and Figs. 3 and 4.

As is seen in Table I and Fig. 2, the agreement of the model with the data is satisfactory for both the threshold data and the total cross sections; $\chi^2/N = 2.9$ for the first part of the fit. Note that this was expected because it was already shown by Cieplý and Smejkal [6] that the chirally motivated separable potential model considering only the S wave reproduces the wide range of low-energy experimental data.

However, the agreement is considerably worse in the P-wave sector. In Fig. 3, the asymmetries in the angular distribution of the differential cross sections A_1/A_0 are shown for all four channels where data are available. Although the experimental data are reproduced sufficiently well in the $\pi^-\Sigma^+$ and $\pi^+\Sigma^-$ channels, the model fails for the K^-p and $\overline{K}^0n$ channels. Note that the sign of the asymmetry is correct, but the absolute value is too small. It suggests that the P-wave potential is too weak.

The notion that the P-wave potential motivated by the $O(p^1)$ chiral Lagrangian is too weak is enforced if one looks at the possible resonance in the $\pi\Sigma$ amplitudes (see Fig. 4). The isoscalar amplitude in the 0^+ partial wave clearly shows a resonant structure, which can be identified with the $\Lambda(1405)$ resonance (as is discussed more extensively in Ref. [6]). On the other hand, in the isovector 1^+ partial wave, where the $\Sigma(1385)$ resonance lies, there is no resonant behavior observed.

To check this hypothesis, the dependence of the $\pi\Sigma$ isovector amplitude on the strength of the P-wave interaction was studied in a simplest possible way. The P-wave potential, Eqs. (22) and (23), was multiplied by the new parameter P_{scale}, which controls the strength of the P-wave interaction, while

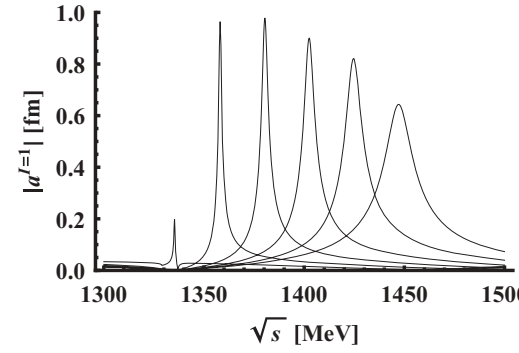

FIG. 5. Absolute values of isovector $\pi\Sigma$ amplitude for 1^+ (right) partial waves obtained with artificially strengthened P-wave interaction. Curves correspond to the values of P_{scale} from -3.9 to -4.4 with peaks moving from left to right. The dashed line corresponds to the $P_{\text{scale}} = 1$.

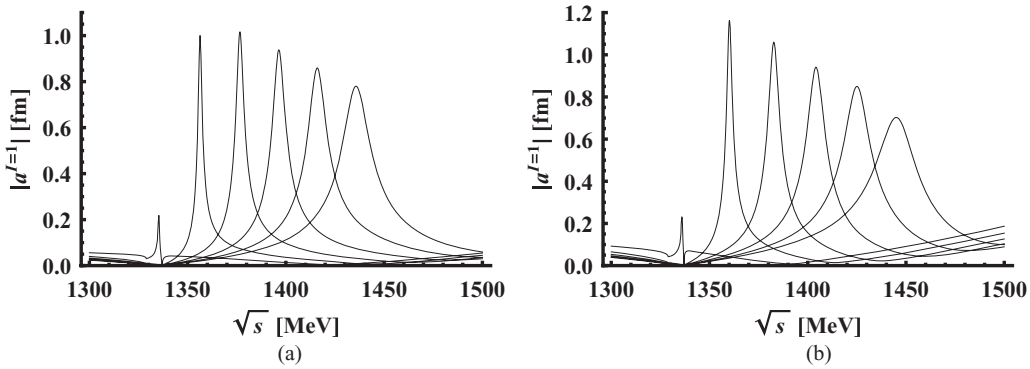

FIG. 6. Absolute values of isovector $\pi\Sigma$ amplitude for 1^+ partial waves obtained with artificially strengthened P-wave interaction. Graph (a) corresponds to $\alpha^P = 1100\,\text{MeV}$ and values of P_{scale} from -6.7 to -7.7. Graph (b) corresponds to $\alpha^P = 900\,\text{MeV}$ and values of P_{scale} from -10.5 to -13.0.

keeping the parameters f_π, α^S, and α^P fixed to the values obtained in the fit. As is seen in Fig. 5, the resonant structure above the $\pi\Sigma$ threshold appears for $P_{\text{scale}}^{\text{RES}} \approx -3.9$ and with increasing strength of the potential moves towards higher energies.

The numerical value of the $P_{\text{scale}}^{\text{RES}}$ where the resonant structure appears depends on the value of α^P. With the decreasing value of inverse range parameter α^P, the absolute value of $P_{\text{scale}}^{\text{RES}}$ increases. Graphs analogous to the one in Fig. 5 for $\alpha^P = 1100\,\text{MeV}$ and $\alpha^P = 900\,\text{MeV}$ are presented in Fig. 6; corresponding values of $P_{\text{scale}}^{\text{RES}}$ are -6.7 and -10.5, respectively.

Note that the model of this paper is based only on the first-order chiral Lagrangian. In their latest version, the model of Cieplý and Smejkal [10] is based on the second-order chiral Lagrangian and has seven free parameters to describe the S-wave physics only. Similarly, a more sophisticated potential containing the P-wave interaction can be developed if one considers a second-order Lagrangian and allows different inverse range parameters for different channels. Such a model could, in principle, be able to capture the desired resonant behavior in the 1^+ partial wave if the respective low-energy constants coming from the second-order chiral Lagrangian were big enough.

The approach using a more sophisticated model, however, leads to a substantial increase in the number of free parameters. Note that there is already a certain level of freedom in the formulation of the model itself. For example, the functional form of the form factors (19) and (20) is not constrained by any underlying theory and the Yamaguchi-type form was chosen for simplicity. The vast space of free parameters combined with the poor quality of the data would make any interpretation of any result obtained quite problematic. On the other hand, better measurements of angular distribution asymmetries or other quantities that would more firmly constrain the P-wave interaction would certainly gain a more firm physical ground to the extended model.

The role of chiral perturbation theory is more subtle in the presented model. Because the $\overline{K}N$ system is outside the regime of validity of χPT—it was the original motivation for an alternative approach in the first place—χPT serves only as a guideline in the construction of the respective potentials. Note, on the other hand, that the very use of χPT for the P-wave physics in the strange sector may raise an important question. It was established phenomenologically [21,30] that the $\Sigma(1385)$ resonance couples strongly to the $\pi\Lambda$ channel, weakly to the $\pi\Sigma$ channel, and negligibly to the $\overline{K}N$ channel. It suggests that the $SU(3)$ flavor symmetry is badly broken and therefore the use of chiral physics may be misguided—even if it serves only as a motivation. Recall, however, that chirally motivated models were successful in the description of various S-wave phenomena in the strange sector and thus the use of chiral physics as a guideline for the construction of P-wave models seems to be a natural extension. From this point of view, the introduction of a new scaling parameter, P_{scale}, which on one hand shifts the model away from χPT and on the other hand improves the agreement with the experimental data, does not seem to be unreasonable.

In summary, it was shown that the model based on the solution of the Lippmann-Schwinger equation with the interaction described by the separable potential (developed in Sec. III) is able to capture the physics of the P-wave interaction. It was also shown that, although working quite well for the S wave, the model based on the chiral Lagrangian at the lowest order (developed in Sec. IV) is not sufficient to even qualitatively reproduce the meson-baryon interaction in the strange sector for the $L = 1$ partial wave. The possible extension of the model that would be based on the $O(p^2)$ chiral Lagrangian is, in principle, possible, but problematic due to the huge amount of new free parameters to consider.

ACKNOWLEDGMENTS

I thank P. Bedaque, A. Cieplý, T.D. Cohen, and A. Gal for valuable discussions and encouragement. This work was supported by the US Department of Energy through Grant No. DE-FG02-93ER-40762.

APPENDIX

The Appendix consists of Tables II–IV, which specify the couplings $\mathcal{C}^{\cdots}_{(ai)\to(bj)}$ among channels.

TABLE II. Coupling matrix $\mathcal{C}^{WT}_{(ai)\to(bj)}$.

	$\pi^0\Lambda$	$\pi^0\Sigma^0$	$\pi^-\Sigma^+$	$\pi^+\Sigma^-$	K^-p	$\overline{K}^0n$	$\eta\Lambda$	$\eta\Sigma^0$	$K^0\Xi^0$	$K^+\Xi^-$
$\pi^0\Lambda$	0	0	0	0	$\sqrt{3}$	$-\sqrt{3}$	0	0	$-\sqrt{3}$	$\sqrt{3}$
$\pi^0\Sigma^0$		0	4	4	1	1	0	0	1	1
$\pi^-\Sigma^+$			4	0	2	0	0	0	2	0
$\pi^+\Sigma^-$				4	0	2	0	0	0	2
K^-p					4	2	3	$\sqrt{3}$	0	0
$\overline{K}^0n$						4	3	$-\sqrt{3}$	0	0
$\eta\Lambda$							0	0	3	3
$\eta\Sigma^0$								0	$-\sqrt{3}$	$\sqrt{3}$
$K^0\Xi^0$									4	2
$K^+\Xi^-$										4

TABLE III. Coupling matrix $\mathcal{C}^{\text{direct}}_{(ai)\to(bj)}$.

	$\pi^0\Lambda$	$\pi^0\Sigma^0$	$\pi^-\Sigma^+$	$\pi^+\Sigma^-$	K^-p
$\pi^0\Lambda$	$4D^2$	0	$-4\sqrt{3}DF$	$4\sqrt{3}DF$	$2\sqrt{3}D(D-F)$
$\pi^0\Sigma^0$		$4D^2$	$4D^2$	$4D^2$	$-2D(D+3F)$
$\pi^-\Sigma^+$			$4D^2+12F^2$	$4D^2-12F^2$	$-2D(D+3F)-6F(D-F)$
$\pi^+\Sigma^-$				$4D^2+12F^2$	$-2D(D+3F)+6F(D-F)$
K^-p					$(D+3F)^2+3(D-F)^2$
	$\overline{K}^0n$	$\eta\Lambda$	$\eta\Sigma^0$	$K^0\Xi^0$	$K^+\Xi^-$
$\pi^0\Lambda$	$-2\sqrt{3}D(D-F)$	0	$4D^2$	$-2\sqrt{3}D(D+F)$	$2\sqrt{3}D(D+F)$
$\pi^0\Sigma^0$	$-2D(D+3F)$	$-4D^2$	0	$-2D(D-3F)$	$-2D(D-3F)$
$\pi^-\Sigma^+$	$-2D(D+3F)+6F(D-F)$	$-4D^2$	$-4\sqrt{3}DF$	$-2D(D-3F)+6F(D+F)$	$-2D(D-3F)-6F(D+F)$
$\pi^+\Sigma^-$	$-2D(D+3F)-6F(D-F)$	$-4D^2$	$4\sqrt{3}DF$	$-2D(D-3F)-6F(D+F)$	$-2D(D-3F)+6F(D+F)$
K^-p	$(D+3F)^2-3(D-F)^2$	$2D(D+3F)$	$2\sqrt{3}D(D-F)$	$D^2-9F^2-3(D^2-F^2)$	$D^2-9F^2+3(D^2-F^2)$
$\overline{K}^0n$	$(D+3F)^2+3(D-F)^2$	$2D(D+3F)$	$-2\sqrt{3}D(D-F)$	$D^2-9F^2+3(D^2-F^2)$	$D^2-9F^2-3(D^2-F^2)$
$\eta\Lambda$		$4D^2$	0	$2D(D-3F)$	$2D(D-3F)$
$\eta\Sigma^0$			$4D^2$	$-2\sqrt{3}D(D+F)$	$2\sqrt{3}D(D+F)$
$K^0\Xi^0$				$(D-3F)^2+3(D+F)^2$	$(D-3F)^2-3(D+F)^2$
$K^+\Xi^-$					$(D-3F)^2+3(D+F)^2$

TABLE IV. Coupling matrix $\mathcal{C}^{\text{crossed}}_{(ai)\to(bj)}$.

	$\pi^0\Lambda$	$\pi^0\Sigma^0$	$\pi^-\Sigma^+$	$\pi^+\Sigma^-$	K^-p
$\pi^0\Lambda$	$4D^2$	0	$4\sqrt{3}DF$	$-4\sqrt{3}DF$	$-\sqrt{3}(D+F)(D+3F)$
$\pi^0\Sigma^0$		$4D^2$	$-12F^2$	$-12F^2$	$3(D+F)(D-F)$
$\pi^-\Sigma^+$			0	$4D^2-12F^2$	0
$\pi^+\Sigma^-$				0	$6(D+F)(D-F)$
K^-p					0
	$\overline{K}^0n$	$\eta\Lambda$	$\eta\Sigma^0$	$K^0\Xi^0$	$K^+\Xi^-$
$\pi^0\Lambda$	$\sqrt{3}(D+F)(D+3F)$	0	$-4D^2$	$\sqrt{3}(D-F)(D-3F)$	$-\sqrt{3}(D-F)(D-3F)$
$\pi^0\Sigma^0$	$3(D+F)(D-F)$	$4D^2$	0	$3(D-F)(D+F)$	$3(D-F)(D+F)$
$\pi^-\Sigma^+$	$6(D+F)(D-F)$	$4D^2$	$-4\sqrt{3}DF$	0	$6(D-F)(D+F)$
$\pi^+\Sigma^-$	0	$4D^2$	$4\sqrt{3}DF$	$6(D-F)(D+F)$	0
K^-p	0	$(D+3F)(D-3F)$	$-\sqrt{3}(D-F)(D-3F)$	$6(D+F)(D-F)$	$D^2-9F^2+3(D^2-F^2)$
$\overline{K}^0n$	0	$(D+3F)(D-3F)$	$\sqrt{3}(D-F)(D-3F)$	$D^2-9F^2+3(D^2-F^2)$	$6(D+F)(D-F)$
$\eta\Lambda$		$4D^2$	0	$(D+3F)(D-3F)$	$(D+3F)(D-3F)$
$\eta\Sigma^0$			$4D^2$	$\sqrt{3}(D+F)(D+3F)$	$-\sqrt{3}(D+F)(D+3F)$
$K^0\Xi^0$				0	0
$K^+\Xi^-$					0

[1] S. Weinberg, Physica A **96**, 327 (1979).
[2] V. Bernard, N. Kaiser, and U. G. Meißner, Int. J. Mod. Phys. E **4**, 193 (1995).
[3] K. Nakamura (Particle Data Group 2010), J. Phys. G **37**, 075021 (2010).
[4] N. Kaiser, P. B. Siegel, and W. Weise, Nucl. Phys. A **594**, 325 (1995).
[5] A. Cieplý and J. Smejkal, Eur. Phys. J. A **34**, 237 (2007).
[6] A. Cieplý and J. Smejkal, Eur. Phys. J. A **43**, 191 (2010).
[7] T. Waas, N. Kaiser, and W. Weise, Phys. Lett. B **365**, 12 (1996).
[8] M. Lutz, Phys. Lett. B **426**, 12 (1998).
[9] A. Cieplý, E. Friedman, A. Gal, D. Gazda, and J. Mareš, Phys. Rev. C **84**, 045206 (2011).
[10] A. Cieplý and J. Smejkal, Nucl. Phys. A **881**, 115 (2012).
[11] V. Krejčiřík, A. Cieplý, and A. Gal, Phys. Rev. C **82**, 024609 (2010).
[12] A. Cieplý, E. Friedman, A. Gal, and V. Krejčiřík, Phys. Lett. B **698**, 226 (2011).
[13] W. Weise and R. Härtle, Nucl. Phys. A **804**, 173 (2008).
[14] D. Gazda and J. Mareš, Nucl. Phys. A **881**, 159 (2012).
[15] M. L. Goldberger and K. M. Watson, *Collision Theory* (Willey & Sons, New York, 1964).
[16] J. A. Oller and U. G. Meißner, Phys. Lett. B **500**, 263 (2001).
[17] B. Borasoy, R. Nißler, and W. Weise, Eur. Phys. J. A **25**, 79 (2005).
[18] P. C. Bruns, M. Mai, and U. G. Meißner, Phys. Lett. B **697**, 254 (2011).
[19] M. Mai and U. G. Meißner, arXiv:1202.2030.
[20] Y. Yamaguchi, Phys. Rev. **95**, 1628 (1954).
[21] A. D. Martin, Nucl. Phys. B **179**, 33 (1981).
[22] M. Bazzi *et al.*, Nucl. Phys. A **881**, 88 (2012).
[23] J. Ciborowski *et al.*, J. Phys. G **8**, 13 (1982).
[24] D. Evans *et al.*, J. Phys. G **9**, 885 (1983).
[25] M. Sakitt *et al.*, Phys. Rev. **139**, B719 (1965).
[26] W. E. Humphrey and R. R. Ross, Phys. Rev. **127**, 1305 (1962).
[27] T. S. Mast *et al.*, Phys. Rev. D **14**, 13 (1976).
[28] R. O. Bangerter *et al.*, Phys. Rev. D **23**, 1485 (1981).
[29] M. B. Watson, M. Ferro-Luzzi, and R. D. Tripp, Phys. Rev. **131**, 2248 (1963).
[30] J. K. Kim, Phys. Rev. Lett. **19**, 1074 (1967).